

MIGRATION AND GROWTH OF PROTOPLANETARY EMBRYOS II: EMERGENCE OF PROTO-GAS-GIANTS CORES VERSUS SUPER EARTHS' PROGENITOR

BEIBEI LIU^{1,2}, XIAOJIA ZHANG³, DOUGLAS N. C. LIN^{2,3,4}, AND SVERRE J. AARSETH⁵

Submitted to the Astrophysical Journal

ABSTRACT

Nearly 15 – 20% of solar type stars contain one or more gas giant planet. According to the core-accretion scenario, the acquisition of their gaseous envelope must be preceded by the formation of super-critical cores with masses ten times or larger than that of the Earth. It is natural to link the formation probability of gas giant planets with the supply of gas and solid in their natal disks. However, a much richer population of super Earths suggests that 1) there is no shortage of planetary building-block material, 2) gas giants' growth barrier is probably associated with whether they can merge into super-critical cores, and 3) super Earths are probably failed cores which did not attain sufficient mass to initiate efficient accretion of gas before it is severely depleted. Here we construct a model based on the hypothesis that protoplanetary embryos migrated extensively before they were assembled into bona fide planets. We construct a Hermite-Embryo code based on a unified viscous-irradiation disk model and a prescription for the embryo-disk tidal interaction. This code is used to simulate 1) the convergent migration of embryos, and 2) their close encounters and coagulation. Around the progenitors of solar-type stars, the progenitor super-critical-mass cores of gas giant planets primarily form in protostellar disks with relatively high ($\gtrsim 10^{-7} M_{\odot} \text{ yr}^{-1}$) mass accretion rates whereas systems of super Earths (failed cores) are more likely to emerge out of natal disks with modest mass accretion rates, due to the mean motion resonance barrier and retention efficiency.

Subject headings: planetary systems – planet–disk interactions – methods: numerical

1. INTRODUCTION

Over the past 2 decades, more than 1700 exoplanets have been discovered and confirmed with radial velocity and transit surveys (Schneider et al. 2011; Wright et al. 2011). A widely accepted hypothesis for their origin is the sequential accretion scenario which assumes heavy elements in protostellar disks condense into grains, later coagulate into planetesimals and merge into protoplanetary embryos (Ida & Lin 2004a). Above a critical mass ($M_c \sim 10M_{\oplus}$), embryos become protoplanetary cores which accrete gas efficiently (Pollack et al. 1996). The fraction of stars containing gas giant planets, η_J , is determined by whether this process can come to completion before gas is severely depleted (over a time scale $\tau_{\text{dep}} \sim 3\text{--}5$ Myr in their natal disks). After correcting for selection effects, existing data suggest $\eta_J \sim 15\text{--}20\%$ around solar type stars (Cumming et al. 2008; Marcy et al. 2008).

In this paper, we discuss the formation probability of embryos with mass $M_p > M_c$. The growth of their progenitor planetesimals evolves from runaway to oligarchic stage (Kokubo & Ida 1998) and it is eventually impeded when they become dynamically segregated (Lissauer 1987) with an isolation mass

$$M_{\text{iso}} \simeq (3/2)M_* (4k_0M_d/3M_*)^{3/2} \quad (1)$$

where $M_d = \pi\Sigma_d r^2$ and Σ_d are the characteristic mass and surface density of planetesimal disk at a radius r , M_{\odot} and M_{\oplus} are the mass of the Sun and Earth respectively, $k_0 (\sim 10)$ is the normalized width of embryos' feeding zone $R_f = k_0 R_R$, $R_R \equiv a[2M_p/(3M_*)]^{1/3}$ and a are their Roche radius and semi major axis respectively. In a minimum mass nebula (MMN) model (Hayashi 1981; Ida & Lin 2004a), the magnitude of M_{iso} is a fraction of M_c at the present location of Jupiter (5 AU).

We suggest that cores with $M_p > M_c$ were assembled in specific disk locations where Σ_d acquired a local maximum value in excess of the power-law distribution in the MMN model. We assume that such concentration of building-block embryos was induced by the tidal interaction with natal disks which led to their type I migration (Goldreich & Tremaine 1979, 1980). It has been suggested that this process may lead to the accumulation of building block material and enhance the growth of embryos (Nelson 2005; Lyra et al. 2010; Paardekooper et al. 2011; Horn et al. 2012; Hellary & Nelson 2012; Pierens et al. 2013).

Based on the past simulations of embryo-disk interaction (Paardekooper et al. (2010, 2011), hereafter PBK10, PBK11), we briefly recapitulate in §2, the dependence of migration direction and speed on the gas surface density (Σ_g) and temperature (T_g) distribution. These simulations place a single embryo in a set of disk models with idealized power-law Σ_g and T_g distributions. With the publically available 2D hydrodynamic FARGO code (Masset 2001), Zhang et al. (2014a,b) (hereafter Z14a, Z14b) carried out simulations to show that embryos do not significantly interfere each others' tidal interaction with the disk and that type I migration indeed induces them to converge to some idealized trapping radius r_{trap} .

¹ Department of Astronomy & Astrophysics, Peking University, Beijing, 100871, China; bbliu1208@gmail.com

² Kavli Institute for Astronomy & Astrophysics, Peking University, Beijing, 100871, China

³ Department of Astronomy and Astrophysics, University of California, Santa Cruz, CA 95064, USA

⁴ Institute for Advanced Studies, Tsinghua University, Beijing, 100086, Beijing, China

⁵ Institute of Astronomy, Cambridge University, Cambridge, UK

In this paper, we are interested in the possibility of collisions and coalescence of multiple embryos. We first use a self-consistent disk model (Garaud & Lin (2007), hereafter GL07) to show the possibility that convergent migration leads them to a transition radius (r_{trans}) between the viscously heated inner and irradiated outer regions of their natal disks. Since embryos' gravity does not significantly modify the disk structure, it is sufficient to assume the disk gas is in a hydrostatic and thermal equilibrium in the direction normal to the disk plane. In hydrodynamic simulations, any steady-state radial distribution of Σ_g can be approximately maintained with an artificially specified viscosity prescription (Z14a). In subsequent studies, we will examine embryos' evolution during the depletion of the disk over a time scale τ_{dep} of 3-5 Myr when \dot{M}_g declines by much larger magnitude than L_* so that $r_{\text{trap}} = r_{\text{trans}}$ decreases from a few AU's to the stellar proximity (Kretke & Lin (2012), hereafter KL12). Such long-term changes in the boundary conditions will pose a challenge for a full scale multi-dimensional hydrodynamic simulation.

In order to carry out the main technical study of this multi-physics, multi-length-scales, and multi-time-scales problem, we construct a Hermite-Embryo scheme. This code combines the calculation of multiple embryos' dynamical interaction (Aarseth 2003) and the evaluation of their tidal interaction with natal disks. Based on the verification that embryo-disk tidal torque is not affected by inference between multiple embryos (Z14a), we separately apply a torque prescription for each embryo (PBK10,11). In the calculation of the torque strength (Γ), we use a self-consistent model (GL07, KL12).

We verify, in §3, that the Hermite-Embryo code reproduces individual embryos' type I migration rate (\dot{a}) and direction found with hydrodynamic simulations. We present simulations with representative disk models. In disks with modest accretion rates ($\dot{M}_g \lesssim 10^{-8} M_\odot \text{ yr}^{-1}$), embryos converge into convoys of super Earth. The migration time-scale ($\tau_a = a/\dot{a}$) is longer than the libration time (τ_{lib}) of some lowest-order mean motion resonances (MMR's). They have a tendency to capture each others' MMR and form a convoy of resonant super Earths (Z14a).

In §4, we show that in disks with high accretion rates ($\dot{M}_g \gtrsim 10^{-7} M_\odot \text{ yr}^{-1}$), torque is sufficiently strong to induce embryos to bypass the mean motion resonance barrier, cross each other's orbits and merge into cores with $M_p > M_c$. We estimate the critical value of \dot{M}_g which separates these outcomes around solar type stars. For this objective, a set of 2D simulations are adequate. Finally in §5, we summarize our results and discuss their implications.

2. MIGRATION OF PLANETS' BUILDING BLOCKS

Our core formation scenario is based on the assumption that they are assembled near $r_{\text{trap}} = r_{\text{trans}}$ where their progenitor embryos congregated through convergent type I migration.

2.1. Availability of planet-building blocks

For initial conditions, we assume the prior emergence of a population of Earth-size embryos through coagulation (Kenyon & Bromley 2009; Dullemond & Dominik 2005;

Garaud et al. 2013), gravitational instability (Goldreich & Ward 1973; Weidenschilling & Cuzzi 1993; Youdin & Shu 2002; Garaud & Lin 2004), streaming instability (Youdin & Goodman 2005), vortice trapping (Johansen & Youdin 2007), or pebble accretion (Lambrechts & Johansen 2012). Provided their growth can bypass several potential barriers such as hydrodynamic drag (Adachi et al. 1976) or collisional fragmentation (Leinhardt & Richardson 2005; Stewart & Leinhardt 2009), they may grow into dynamically segregated embryos with isolation mass M_{iso} shown in Eq. [1].

Due to uncertainties in the opacity law, it is difficult to reliably extract from observations the value of Σ_d . But, the gas accretion rate \dot{M}_g can be obtained from the UV veiling and spectroscopic data. The diffusion stability of accretion disks requires Σ_g to be an increasing function of \dot{M}_g (Pringle 1981). Any assumed $\Sigma_d - \dot{M}_g$ correlation would require an additional assumption: the dispersion in the metallicity of the disk gas (Z_d) is much smaller than that of \dot{M}_g . It is tempting to extrapolate a dispersion in Σ_d from the observed range of \dot{M}_g ($\sim 10^{-6} - 10^{-10} M_\odot \text{ yr}^{-1}$) among classical T Tauri stars (Hartmann et al. 1998) and to assume that gas giants are formed in disks with high Σ_d and \dot{M}_g 's.

An alternative minimum planetary building block scenario is to extrapolate a population of Earth mass embryos from the Kepler data (Batalha et al. 2013). After taking into account its well understood observational selection effects (Dong & Zhu 2013), transit search with this data set of controlled targets reveals the common existence of super Earth candidates with sizes in the range of $R_p \simeq 1 - 4R_\oplus$ where R_\oplus is the Earth's radius. A vast majority of these multiple-planet systems are most likely to be genuine planets (Lissauer et al. 2012). Follow-up radial velocity (RV) surveys (Marcy et al. 2014) and mass determination from the observed transit timing variations (TTV's) (Wu & Lithwick 2013) have confirmed that: 1) the fraction of stars (η_E) which harbor one or more super Earth candidates is much higher than η_J (Mayor et al. 2011; Howard et al. 2012; Fressin et al. 2013), and 2) in contrast to the observed correlation (Fischer & Valenti 2005; Santos et al. 2004; Johnson et al. 2010) between η_J and the metallicity of their host star (Z_*), the magnitude of η_E appears to be independent of Z_* and M_* (Wang & Fischer 2013; Buchhave et al. 2012, 2014).

In the most up to date Kepler data release, there are 348 confirmed multiple-super Earth systems with $M_p < 100M_\oplus$ and $N \geq 2$. Among them, 119 systems contain $N \geq 3$ members. Their confirmation is based on the upper mass limits obtained with the follow-up RV surveys or TTV measurements. There are another 792 additional multiple Kepler objects of interests (KOI's) listed in the NASA Exoplanet Archive. All but 66 of these unconfirmed KOI's contain solely planetary candidates with $R_p < 10R_\oplus$. Follow-up observations of these KOI's are needed to establish their planetary identity and to determine of their mean composition (Wolfgang & Lopez 2014).

We plot the distribution of individual planets' M_p and the total masses M_s of multiple planetary systems for the 348 confirmed Kepler multiple planetary systems (Fig.

1). Although the mass of some Kepler planets have been obtained with the RV or TTV measurements, most others do not have any measured dynamical information. We extrapolate their M_p from a mass-radius relation

$$R_p \simeq (M_p/M_\oplus)^{1/2.06} R_\oplus. \quad (2)$$

which is empirically fitted to the solar system planets (Lissauer et al. 2011).

Figure 1 shows that even though some individual super Earths may have extrapolated density lower than that of the Earth and $M_p < M_c (\simeq 10M_\oplus)$, the total mass M_s of most multiple KOI systems around individual host stars exceeds M_c . The total available building block materials in many multiple systems are enough to form the critical mass cores, but most of them do not evolve into gas giant planets. We interpret these data to imply that the lack of gas giants around most solar type stars may be due to the inability for sufficient fraction of all available building block materials to be collected into a few cores (with $M_p \geq M_c$) rather than a lack of heavy elements in their natal disks. Based on this inference, we investigate the formation efficiency of cores.

In order to minimize the diverse statistical bias introduced by various survey methods, Figure 1 contains only Kepler's confirmed multiple planets. However, similar mass distributions are obtained with either all 792 unconfirmed KOI's or with all known multiple-planet systems including an additional 95 multiple planet systems which were discovered by RV or ground-based transit surveys.

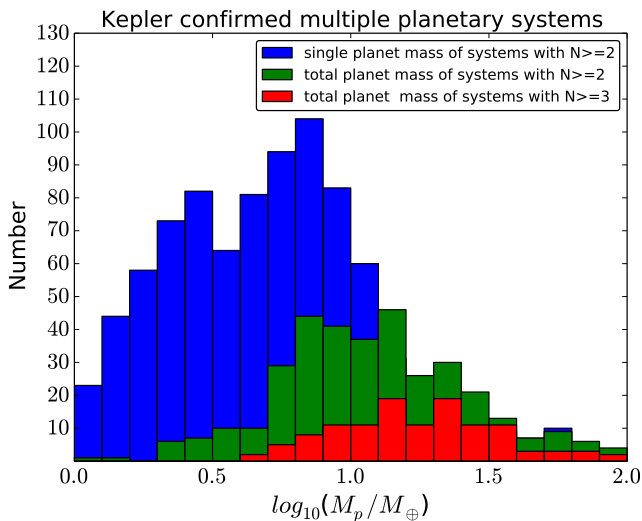


FIG. 1.— The planet mass distribution of multiple exoplanetary systems in confirmed Kepler sample. Blue, green, red lines represent single planet's mass (M_p) in multiple systems with $N \geq 2$, total planetary system's mass (M_s) in multiple systems with $N \geq 2$ and with $N \geq 3$ respectively. The masses are extrapolated from R_p with Eq. [2]).

2.2. Embryos' type I Torque Formulas

Embryos do not have sufficient mass to significantly perturb the disk structure (Lin & Papaloizou 1993). But they can excite waves near their Lindblad and corotation resonances. Based on the assumption that these waves are dissipated as they propagate through the disk, they lead to Lindblad and corotation torque which induces

their migration. Past simulations (PBK10, 11) showed that embryos' migration rate and direction depend on the Σ_g and T_g distributions. We first describe the analytic approximation of the embryo-disk torque.

Linear wave analysis indicate that there is an imbalance in the torque exerted by isolated embryos at their Lindblad resonance on the disk region interior and exterior to their orbits (Tanaka et al. 2002). The net differential Lindblad torque generally causes embryos to undergo inward migration. Embryos also impose corotation torque on the disk gas which follows the horseshoe stream lines. With small speeds relative to the embryos, gas in this region interacts strongly with them. The sign of the corotation torque is determined by the local vortensity ($\zeta = \Sigma_g/\Omega$) of the gas. The net (Lindblad plus corotation) residual torque determines the direction and speed of type I migration.

In an inviscid disk, the initial local vortensity and entropy gradient are erased along the horseshoe stream lines as gas is mixed within a few libration periods (Balmforth & Korycansky 2001). This effect leads to the saturation (weakening) of corotation torque. The angular momentum transport induced by disks' turbulent Reynold's stress leads to both angular momentum and entropy diffusion and the retention of their intrinsic distribution. The competition between planets' gravitational perturbation on the nearby stream lines and the mass flow across the corotation region can be easily captured with an idealized linear analytic treatment.

Extensive 2D numerical simulations (PBK10, 11) of tidal interaction between isolated planets in disks with intrinsic power-law surface density and temperature distributions ($\Sigma_g \propto r^s$ and $T_g \propto r^\beta$) have provided a data base to parameterize the net torque into the following form

$$\Gamma = f_\Gamma(s, \beta, p_\nu, p_\chi) \Gamma_0 \quad (3)$$

where the magnitude of the linear torque expression is

$$\Gamma_0 = (q/h)^2 \Sigma_p r_p^4 \Omega_p^2. \quad (4)$$

Here $q = M_p/M_*$ is the mass ratio between the embryo and its host star, and $h = H/r_p$ is the aspect ratio between the disk thickness ($H = (R_g T/\mu)^{1/2}/\Omega_p$) and the location of the planet $r_p = a$.

The maximum value and sign of the torque coefficient f_Γ are determined by s and β . It includes the sum of all components of the Lindblad and corotation torque. The full strength of the corotation torque is determined by the ζ gradient which is a function of s and β and the extent of its saturation is determined by the dimensionless parameters $p_\nu = (2/3)(R_e x_s^3)^{1/2}$ and $p_\chi = (R_e x_s^3/P_t)^{1/2}$ where $R_e \equiv \Omega_k r_p^2/3\pi\nu$ and $P_t \equiv \nu/\xi$ are the Reynolds and Prandl numbers respectively, ν and ξ are the viscous and radiative diffusion coefficients respectively, and $x_s \simeq (q/h)^{1/2}$ is the dimensionless width of the horseshoe regions. Mass and entropy rapidly diffuse through the narrow horseshoe region of low-mass embryos (with small p_ν and p_χ) such that their torque only affect the gas which u-turns very close to their azimuthal location. In contrast, diffusion cannot cross the wide horseshoe region of high-mass embryos (large p_ν and p_χ) within the libration time scale on the horseshoe orbit. Consequently, the disk's intrinsic vortensity gradient is effectively erased in

this region and the corotation torque is saturated. Maximum corotation torque is exerted by embryos with $p_\nu \sim 1$ or $p_\chi \sim 1$.

Accretion disk models provide values for s , β , Σ_g , T_g , h , ν , ξ , R_e , and P_t (see §2.3). Therefore we can evaluate x_s , p_ν , p_ξ , f_Γ , and total torque Γ_{tot} for embryos with mass M_p at location $r_p (= a)$. The total torque leads to a net change in the semi major axis at rate

$$\frac{da}{dt} = \frac{2f_a q}{h^2} \frac{\Sigma_g r_p^2}{M_*} r_p \Omega_k \quad (5)$$

where $\Gamma_{\text{tot}} = f_a \Gamma_0$ and $f_a = \sum f_{\Gamma,i}$, the index i refers to different torque components including differential Lindblad (f_{Lb}), linear and nonlinear horseshoe and corotation torque. In principle, the inner and outer Lindblad resonances of embryos located near r_{trans} are located in regions of the disks with different values of s and β . But the separation between these resonances and the width of the corotation region are much smaller than both a and the scale length over which s and β changes (Z14b). It is adequate to adopt a smoothing function for the transition of s and β and use the value of $f_{\Gamma,i}$ at $r_p = a$. We can also obtain the rate of change in eccentricity

$$\frac{1}{e} \frac{de}{dt} = \frac{2f_e q}{h^4} \frac{\Sigma_g r_p^2}{M_*} \Omega_k \quad (6)$$

where we assume both inner and outer Lindblad torque lead to eccentricity damping so that $f_e = \sum |f_{\Gamma,i}|$ (Goldreich & Tremaine 1980; Artymowicz 1993; Goldreich & Sari 2003).

2.3. A Self-Consistent Model of Evolving Protostellar Disks

The Σ_g distribution is determined by the efficiency of angular momentum transfer (Lynden-Bell & Pringle 1974; Ruden & Lin 1986). The dominant angular momentum transfer mechanism in accretion disks is turbulent-induced viscous stress (Shakura & Sunyaev 1973). The most likely cause for turbulence in inner (< 0.1 AU) regions of protostellar disks is magnetorotational instability (Balbus & Hawley 1991). Between $\sim 0.1 - 10$ AU, there is a dead zone where the ionization fraction is low and the field cannot diffuse through near the disk midplane. But, MHD turbulence is prevalent in the disk surface layer which is ionized by the stellar irradiation and cosmic rays (Gammie 1996).

For our application, we need to carry out simulations over $10^5 - 6$ orbits. It is computationally practical to construct a relatively simple disk model which robustly reproduces the generic outcomes of embryos' type I migration and apply it to the Hermite-Embryo code. We adopt a self-consistent disk model of Garaud & Lin (2007) (hereafter GL07) based on the assumption that the inner region of the disk is heated by viscous dissipation whereas the outer region is heated by stellar luminosity (L_*). For these models, r_{trap} coincides with the transition radius r_{trans} which separates these two regions (KL12).

Based on the conventional α prescription for viscosity, we assume

$$\nu = \alpha_\nu C_s H = \alpha_\nu R_g T_g / \mu \Omega_k \quad (7)$$

where H is the scale height in the direction normal to the disk plane, R_g and μ are gas constant and molecular

weight. Typical magnitude for the dimensions turbulent efficiency factor $\alpha_\nu \sim 10^{-3}$. In the layered regions, the efficiencies of angular momentum transfer, mass and entropy diffusion are miniscule at the midplane and modest near the surface of the disk. This height (z) dependent structure can be approximated by the standard value of $\alpha_\nu (\sim 10^{-3})$ for the surface layer ($\alpha_H \sim \alpha$ at $z \sim H$) and an order of magnitude smaller value ($\alpha_M \sim 0.1\alpha$) for the midplane region beneath the partially ionized layer.

For computational simplicity, the disk model we adopt in this paper is based on the assumption that it evolves in a quasi steady state in which $\dot{M}_g (= 3\pi\Sigma_g\nu)$ is independent of radius but declines exponentially over the gas depletion time scale such that

$$\dot{M}_g = \dot{M}_0 e^{-t/\tau_{\text{dep}}} \quad (8)$$

with $\tau_{\text{dep}} \sim 3 - 5$ Myr.

In §3 and §4, we show that a critical criterion for the formation of super-critical cores is sufficiently high \dot{M}_g or Σ_g . Since \dot{M}_g monotonically declines, the value of \dot{M}_g during the early epoch of embryo formation determines the outcome of the migration and merger process. For stable accretion disk models, the viscous diffusion time scale generally increases with the disk radius such that their inner regions generally establishes a quasi equilibrium state. We are mostly interested in disk regions not much beyond r_{trap} (a few AU's), a quasi steady state would be established if disks extend well beyond ~ 10 AU (Birnstiel & Andrews 2014). For simulations which indicate that the migration time scale is a fraction of τ_{dep} (see §3 and §4), we do not expect the disk structure to evolve significantly during embryos' migration.

Based on these prescriptions and an idealized opacity law in which $\kappa = \tilde{\kappa}_0 T_g$, GL07 obtained $\Sigma = \Sigma_0 r_{AU}^s$ and $T_g = T_0 r_{AU}^\beta$, where $r_{AU} = (r/1\text{AU})$, with

$$\Sigma_0 = 240 \alpha_3^{-3/4} \kappa_0^{-1/4} m_*^{1/8} \dot{m}_9^{1/2} \text{ g cm}^{-2}, \quad (9)$$

$$T_0 = 120 m_*^{3/8} \dot{m}_9^{1/2} \alpha_3^{-1/4} \kappa_0^{1/4} \text{ K}, \quad (10)$$

$s = -0.375$ and $\beta = -1.125$ for the viscously heated inner region. In the above expression, the normalized quantities, $\alpha_3 \equiv \alpha_\nu / 10^{-3}$, $m_* \equiv M_*/M_\odot$, $\dot{M}_g \equiv \dot{M}_g / (10^{-9} M_\odot \text{ yr}^{-1})$ and $\kappa_0 \equiv \tilde{\kappa}_0 / 0.02$. The opacity κ is in units of $\text{cm}^2 \text{ g}^{-1}$ and likely to be correlated with disk metallicity (Z_d). The corresponding aspect ratio

$$h = 0.025 m_*^{-5/16} \dot{m}_9^{1/4} \alpha_3^{-1/8} \kappa_0^{1/8} r_{AU}^{-1/16} \quad (11)$$

implies this region of the disk is self shadowed.

In the limit of relatively large $\dot{M}_d (> 10^{-8} M_\odot \text{ yr}^{-1})$, the transition from viscous dissipation to surface irradiation takes place in regions where the disk is opaque to either incident stellar irradiation or reprocessed radiation (or both). Using a self consistent treatment of the h distribution, GL07 show that this region is relatively confined. Outside this transition region, the disk becomes optically thin and T_g there can be approximated by the local equilibrium temperature

$$\frac{A_s}{2} \frac{L_*}{4\pi r^2} = \sigma T_e^4, \quad (12)$$

where T_e is the disk's effective temperature, σ is the radiation constant, A_s is the grazing angle of the disk, which can be expressed as $A_s \propto r d(H/r)/dr$. In this limit,

$$\Sigma_0 = 95 m_*^{9/14} \dot{m}_9^{-2/7} \alpha_3^{-1} \text{ g cm}^{-2}, \quad (13)$$

$$T_0 = 300 l_*^{2/7} m_*^{-1/7} \text{ K} \quad (14)$$

with $s = -15/14$, $\beta = -3/7$, and $l_* = L_*/L_\odot$. There is no explicit dependence on κ_0 for Σ_0 and T_0 in this region. For computational simplicity, we neglect the opaque region and determine the transition (trapping) radius

$$r_{\text{trans}} \simeq 0.26 m_*^{0.74} l_*^{-0.41} \dot{m}_9^{0.72} \alpha_3^{-0.36} \kappa_0^{0.36} \text{ AU} \quad (15)$$

by matching T_g from the viscously heated and the optically thin regions.

In this model, all the structural parameters, including s , β , Σ_g , T_g , h , and ν , are functions of M_* , \dot{M}_g , r , and α_ν . In the dissipation-dominated inner disk region, we assume that turbulent mass and heat transport would yield a unit effective Prandtl number (ie $P_t \simeq 1$). This approximation simplifies the evaluation of p_χ .

2.4. Embryos' Migration through Protostellar Disks

We now combine the disk model with the torque formula, neglecting any feedback on the disk structure (KL12). This approximation is justified by previous hydrodynamic simulations especially for embryos with $R_R < H$ (Lin & Papaloizou 1986b; Paardekooper et al. 2010; Zhang et al. 2014b).

For very low-mass (with $p_\nu \ll 1$) and high-mass (with $p_\nu \gg 1$) embryos, corotation torque is highly saturated and only differential Lindblad torque in equation (6) contribute to the total torque such that

$$f_{Lb} = 1.7\beta - 0.1s - 2.5 \quad (16)$$

is negative in both the inner and outer disk regions. In this limit, embryos would migrate inward until they reach the inner boundary of the disk.

In the irradiated outer regions of the disk, embryos migrate inward even when the corotation torque operates at full strength. But for the viscously heated inner region, the fully unsaturated corotation and horseshoe torque is not only stronger than the Lindblad torque but also induces embryos to migrate outward. However the full strength of the corotation torque Γ_{cr} can only be realized for embryos with a range of masses (KL12). In the viscously heated inner regions of the disk, the optimum mass for embryos' outward migration is obtained from the requirement $p_\nu \sim 1$ (or $p_\xi \sim 1$). From the expression for p_ν , p_ξ , equations (7) and (11), we find

$$M_{\text{opt}} \simeq m_*^{13/48} \dot{m}_9^{7/12} \alpha_3^{3/8} \kappa_0^{7/24} r_{\text{AU}}^{-7/48} M_\oplus. \quad (17)$$

There is a tendency for embryos with $M_p \sim M_{\text{opt}}$ to migrate and converge to r_{trans} . The location of r_{trans} depends on both \dot{M}_g and L_* (see eq. [15]). In equation (17) M_{opt} depends on \dot{M}_g and M_* more sensitively than on r (see further discussions in the next section). In the standard α disk model, the range of M_p (around M_{opt}) which can avoid saturation of corotation torque and enable outward migration (Baruteau & Masset 2013) is

$$0.32 q^{3/2} h^{-7/2} \leq \alpha_\nu \leq 0.16 q^{3/2} h^{-9/2}. \quad (18)$$

The ratio between the upper and lower mass limits ($\sim (2h)^{-2/3}$) is generally a few. In the derivation of the above mass range, the magnitude of α_ν is assumed to be independent of the distance z above the midplane. However, the width of low-mass embryos' horseshoe region ($x_s r$) is smaller than the thickness (H_{dead}) of the dead zone beneath the disk's active surface layer. From equation (18) we find that a small α_M (appropriate for the disk midplane) would substantially reduce the lower limit in the mass range of embryos with unsaturated corotation torque (KL12). Although embryos with $M_p < M_\oplus$ may have a positive f_a , their $\tau_a > \tau_{\text{dep}}$ due to the M_p dependence in Γ_0 (Eq. [4]).

We now check for self consistency of our no feedback assumption. A necessary condition for embryos to induce sufficiently strong perturbation is to open a gap (Lin & Papaloizou 1986a) is $R_R > H$. For optimum-mass embryos,

$$\frac{R_R(M_{\text{opt}})}{H} \sim 0.5 m_*^{5/72} \dot{m}_9^{-1/18} \alpha_3^{1/4} \kappa_0^{-1/36} r_{\text{AU}}^{1/72} \quad (19)$$

such that gap formation may be marginally avoided as numerical simulations have shown.

2.5. The Hermite-Embryo numerical scheme

The torque prescription constructed by PBK10 is for single power-law Σ_g and T_g distribution. In our disk model, the values of s and β change across r_{trans} . Hydrodynamic simulations show that the strength and sign of the torque are not significantly modified by this more complex disk structure (Z14b).

The torque prescription is an approximation of the tidal interaction between isolated embryos and their natal disks. As the embryos converge, their horseshoe regions overlap. The perturbation by neighboring embryos may modify the gas stream lines and the saturation condition. Detailed 2D hydrodynamic simulations show that such interference does not significantly modify the corotation torque and the prescription derived for isolated embryos continues to provide adequate approximation for a system of converging embryos (Z14b).

Based on these justifications, we modify an N-body HERMIT4 code (Aarseth 2003) and construct a Hermite-Embryo code to include the effect of embryos-disk interaction. Gravitational interaction between representative embryos is calculated with a time-symmetric scheme of Kokubo & Ida (1998) and the Burdet-Heggie regularization (discussed in Aarseth 2003) is applied for the treatment of close encounters. These features enable efficient and reliable integration of embryos dynamics on time scales comparable to τ_{dep} (a few Myr).

Separate disk torque on individual embryos are added to the equation of motion such that

$$\frac{dv_\theta}{dt} = \frac{\Gamma_{\text{tot}}}{M_p r}, \quad (20)$$

$$\frac{dv_r}{dt} = -\frac{v_r}{\tau_e}. \quad (21)$$

The migration timescale is then given by

$$\tau_a \simeq \frac{a}{\dot{a}} = M_p \sqrt{(GM_* a)} / (2f_a \Gamma_0). \quad (22)$$

TABLE 1
THE PROPERTIES OF ADOPTED MODELS

Model	Accretion rate \dot{M} ($M_\odot \text{ yr}^{-1}$)	viscous α	include dead zone
A	7×10^{-9}	10^{-3}	NO
B	10^{-7}	10^{-3}	NO
C	10^{-7}	10^{-3}	YES

Model	number of planets (N_p)	planet Mass (M_\oplus)	include planet-disk interaction
A1	15	2.0	YES
A2	4	10.0	YES
B1	2 (inner) +5 (outer)	5.0 (inner)+4.0 (outer)	YES
B2	2 (inner) +5 (outer)	5.0 (inner)+4.0 (outer)	NO
C1	15	2	YES

where a negative value for f_a implies orbital decay. The timescale for eccentricity damping timescale is a factor of $(1/h)^2$ shorter (Tanaka et al. 2002; Kley & Nelson 2012) than the orbital decay timescale:

$$\tau_e \simeq \frac{e}{\dot{e}} = h^2 M_p \sqrt{(GM_* a)} / (2f_e \Gamma_0), \quad (23)$$

where f_e is the coefficient for total Lindblad and corotation torque, v_θ and v_r are the velocity in azimuthal and radial direction.

The Hermite-Embryo code is well suited to simulate embryos' long-term interaction with each other and their natal disks. It can reproduce MMR capture and treat close encounters between multiple embryos. For comparison with previous results in Z14a and Z14b, all the models presented in this paper are simulated in the 2D limit. This approximation does not affect the condition for MMR capture. But it does reduce the collision frequency. During episodes when two embryos' separation becomes smaller than the sum of their physical radii (R_p obtained from equation (2)), we assume they merge with conservation of total mass and angular momentum. In the 3D limit, the collision time scale is given by equation (2). But in the 2D (mono-layer) approximation τ_c is smaller by the reduction factor $f_{2/3D}$. Currently, we neglect a small amount of angular momentum transfer between the embryos' spin and orbit. This effect will be examined in a future follow-up study.

3. EMERGENCE OF RESONANT SUPER EARTHS

3.1. Preferential Destiny of Migrating Embryos

Applying the disk model (GL07) into the torque prescription (PBK10, 11), we determine the coefficients f_r , f_a and f_e of the total type I torque, migration, and circularization rates. Two panels in Figure 2 show the radial distribution of f_a for different mass embryos. The black dashed line denotes r_{trans} . In the irradiated regions exterior to the black line, $f_a < 0$ and embryos of all masses migrate inward. In the viscously heated inner region (interior to the black line), corotation torque, at its full strength, dominates the differential Lindblad torque and induces embryos to migrate outward. However, we can use the PBK10 prescription to show that only within a limited range of M_p around M_{opt} (Eq. [18]), embryos migrate outward because their corotation torque is not severely saturated.

In Figure 2, the disk parameter for model A is $\dot{M}_g = 7 \times 10^{-9} M_\odot \text{ yr}^{-1}$, whereas for model B it is $\dot{M}_g = 10^{-7} M_\odot \text{ yr}^{-1}$. In both models, $\alpha_\nu = 10^{-3}$ and

$M_* = 1M_\odot$. These parameters are chosen to respectively represent the advanced and active phases of disk evolution. For model A (left panel), embryos interior to $r_{\text{trans}} = 1.05 \text{ AU}$ and with $M_p \sim 2 - 9M_\oplus$ migrate outward. For model B (right panel), $r_{\text{trans}} = 7.10 \text{ AU}$. Interior to r_{trans} , embryos with mass in the red region (i.e. $M_p \sim 5 - 25M_\oplus$) migrate outward. Both the optimum mass and mass range are in good agreement with the values estimated with equations (17) and (18). In a minimum mass nebula, M_{iso} is around a few M_\oplus which falls within the outwardly migrating range in Figure 2 and these embryos have a tendency to migrate to and accumulate near r_{trans} .

3.2. Convoys of super Earths trapped in MMR

In order to examine embryos' concurrent interaction with each other and with their natal disk, we use the Hermite-Embryos code to compute the dynamical evolution of multiple embryos. Based on the boundary conditions in models A and B, we present the results of two series of simulations.

In model A1, we adopt 15 equal-mass ($M_p = 2M_\oplus$) embryos. They are initially separated by $k_0 = 10$ with a in the range of 0.4–3.1AU. During the oligarchic growth, the embryos' isolation mass

$$M_{\text{iso}} \simeq 0.16 \left(\frac{\Sigma_d}{10 \text{ g cm}^{-2}} \right)^{3/2} \left(\frac{r}{1 \text{ AU}} \right)^3 \left(\frac{M_*}{1 M_\odot} \right)^{-1/2} M_\oplus. \quad (24)$$

Assuming a uniform normalized metallicity Z_d in the disk (with respect to the solar composition) for the viscously heated inner region, we find from equation (9),

$$M_{\text{iso}} \simeq 0.16 Z_d^{3/2} \kappa_0^{-3/8} \alpha_3^{-9/8} m_*^{-5/16} \dot{m}_{-9}^{3/4} r_{\text{AU}}^{39/16} M_\oplus. \quad (25)$$

Note that κ_0 is a function of metallicity in micron grains whereas Z_d is metallicity in condensed heavy elements.

The initial values of M_p in model A1 are self consistent with the disk parameters at the chosen location. All the embryos are assumed to be coplanar and their initial eccentricities follow a Rayleigh distribution

$$p(e) = \frac{e}{\sigma_0^2} \exp\left(-\frac{e^2}{2\sigma_0^2}\right), \quad \sigma_0 = 0.02. \quad (26)$$

Other orbital elements (argument of periastron, longitude of ascending node and mean anomaly) are chosen randomly from $0^\circ - 360^\circ$.

The orbital evolution of these systems are all computed less than 5×10^5 yrs. Since this is shorter than the disk

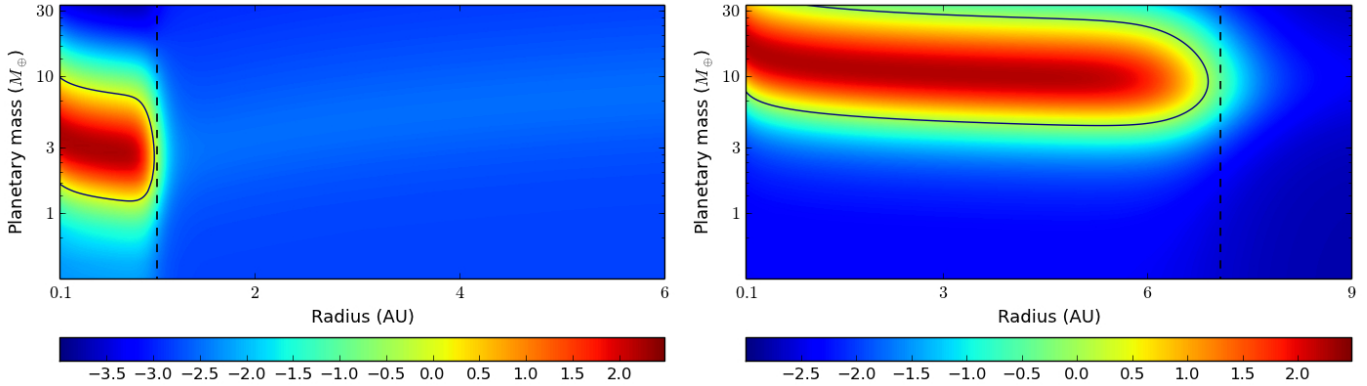


FIG. 2.— The type I migration coefficient (f_a) for a range of embryos' mass at different location of the disk. Black dashed line represent the transition radius r_{trans} . **Left:** model A with $\dot{M} = 7 \times 10^{-9} M_{\odot}/\text{yr}$, $\alpha_{\nu} = 10^{-3}$, $\Sigma_0 = 635 \text{g/cm}^2$ and $r_{\text{trans}} = 1.05 \text{AU}$. **Right:** model B with $\dot{M} = 1 \times 10^{-7} M_{\odot}/\text{yr}$, $\alpha_{\nu} = 10^{-3}$, $\Sigma_0 = 2400 \text{g/cm}^2$ and $r_{\text{trans}} = 7.10 \text{AU}$.

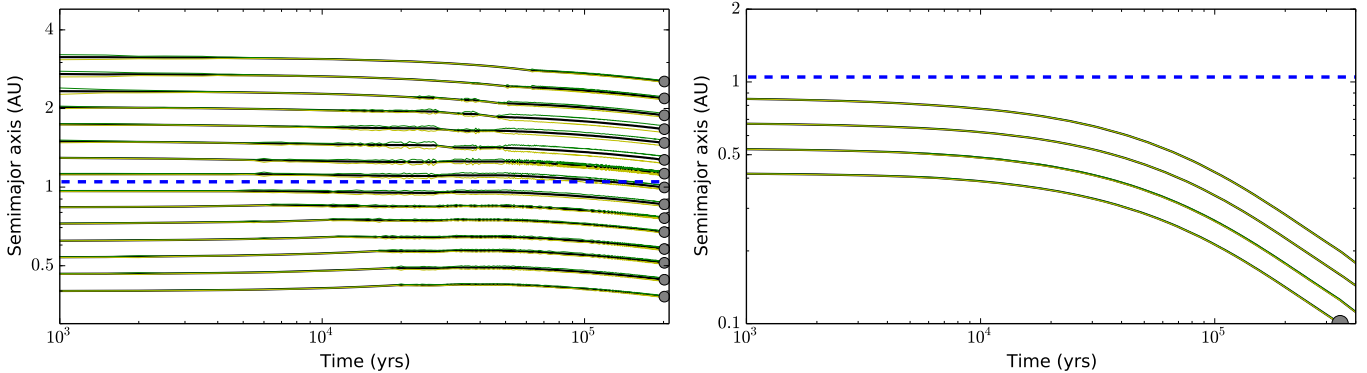


FIG. 3.— The mutual interaction between embryos and their natal disks. The black lines trace the evolution of embryos' semi-major axis and blue dashed line indicates the location of r_{trap} . Green and yellow lines are embryos' apocentre and pericentre distance. Disk parameters are chosen to be those of model A. **Left** model A1: A system of fifteen $2M_{\oplus}$ embryos which are initially separated by $10R_{\text{R}}$ between $0.6 - 3.7 \text{AU}$. **Right** model A2: A system of four $10M_{\oplus}$ embryos which are initially separated by $10R_{\text{R}}$ between $0.43 - 0.83 \text{AU}$.

depletion time scale, we adopt a steady state disk model. But, in all our models, the computed time is adequately long to simulate the embryos' migration and their potential collisions.

Embryos' migration of Model A1 is plotted in the left panel of Figure 3. They undergo convergent migration on a time scale of $\sim 6 - 8 \times 10^4$ yr as expected. However, their migration is stalled when they capture each other into their mutual MMR's. Although the total mass of the embryos ($30M_{\oplus}$) exceeds M_c ($\sim 10M_{\oplus}$) required for the onset of gas accretion, they form a compact convoy of super Earths with non intersecting orbits. The grey dots in Figure 3 are plotted at the endpoint evolution of each embryos, which is proportional to the mass of embryos.

3.3. Embryos' MMR Capture Condition

The theory of MMR capture has been extensively developed by Peale (1976) and Murray & Dermott (1999) (hereafter MD). A necessary condition for MMR capture is that the time scale $\tau_{\Delta a}$ ($\sim \Delta a_{\text{res}}/\dot{a}$) for migration through their characteristic width (Δa_{res}) is longer than their libration time scale $\tau_{\text{lib}} \sim (qf_{\text{res}}e_{\text{res}})^{-1/2}n^{-1}$, where n is orbital mean motion and $f_{\text{res}} = \alpha_a f_d(\alpha_a)$ (where f_d is a function of the semi major axis ratio α_a) from Eq. 8.47 in MD. Within Δa_{res} , an equilibrium eccentricity (e_{res}) is maintained by a balance between its excitation

during embryos' resonant migration

$$e\dot{e}_{\text{exc}} \sim \dot{a}/a \sim 1/\tau_a \quad (27)$$

(see Eq. 8.37 in MD) and its damping due the embryo-disk torque $\dot{e}_{\text{damp}} \sim e/\tau_e$ such that $e_{\text{res}} \sim (\tau_e/\tau_a)^{1/2} \sim h$ (see Eqs. [22] and [23]). From equation (8.58) in MD, we deduce

$$\Delta a_{\text{res}} \sim (qf_{\text{res}}e_{\text{res}})^{1/2}a \sim (qf_{\text{res}}h)^{1/2}a \quad (28)$$

$$\tau_{\text{lib}} \sim (a/\Delta a_{\text{res}})P/2\pi. \quad (29)$$

With these dependencies, MMR's capture condition $\tau_{\Delta a} > \tau_{\text{lib}}$ is reduced to

$$\Sigma_g r^2 < \Sigma_{\text{res}} r^2 \simeq f_{\text{res}} h^3 M_*, \quad (30)$$

which is independent of embryos' mass. In the above expression, Σ_{res} is defined to be the critical surface density for resonant capture.

The magnitude of f_{res} is the order of a few and it decreases with α_a (i.e. f_{res} is smaller for 3:2 than 2:1 resonance) such that it is possible for two embryos to enter into their 3:2 MMR even though they have failed to do so at their 2:1 MMR (Z14a). In the proximity of r_{trans} , we find (from eqs. [9], [15] and [30]) that,

$$\Sigma_g(r_{\text{trans}})r_{\text{trans}}^2 \simeq \dot{m}_g^{1.67} m_*^{1.33} l_*^{-0.67} \alpha_3^{-1.34} \kappa_0^{0.34} M_{\oplus}. \quad (31)$$

with the critical condition for resonant trapping to be

$$\dot{m}_g \simeq 6f_{\text{res}}^{0.95} m_*^{-1.33} \alpha_3^{0.97} \kappa_0^{-0.026} l_*^{0.70}. \quad (32)$$

This analytic approximation confirms that during their convergent migration, embryos embedded in disks with relatively low \dot{M}_g are likely to capture each other onto their MMR's. This inference is consistent with the results in numerical model A1. In this consideration, *the suppression of gas giant planet formation is due to the inability for embryos to merge rather than merely an inadequate supply of building block material.*

3.4. Limited Gas Accretion

Prior to the onset of efficient gas accretion, embryos with $M_p < M_c$ can accrete gas, albeit on a Kelvin-Helmholtz cooling time scale τ_{KH} . For grain opacity with a solar metallicity, $\tau_{\text{KH}} \sim 10^9 (M_p/M_\oplus)^{-3}$ yr (Pollack et al. 1996; Ida & Lin 2004a). In the limit that $\tau_{\text{KH}} > \tau_{\text{dep}}$, embryos may accrete envelopes with mass $M_{\text{env}} \sim M_p \tau_{\text{dep}} / \tau_{\text{KH}} \sim (M_p/M_\oplus)^4 (\tau_{\text{dep}}/1 \text{ Gyr}) M_\oplus$ before the gas is depleted in the disk. Due to energetic impacts between embryos and residual planetesimals, this envelope mass may not be retained. These diverse outcomes may contribute to the observed dispersion in the density of super Earths (Wu & Lithwick 2013).

The above consideration indicates that cores' M_p need to exceed M_c for them to evolve into gas giants before disk depletion. Equation (17) indicates that M_{opt} is an increasing function of \dot{M}_g . For the disk parameters in model A1, $M_{\text{opt}} < M_c$ such that the embryos' corotation torque is saturated before they evolve into cores. We introduce model A2 to illustrate this inference. Four $10M_\oplus$ embryos are placed in a disk with identical parameters as those in model A1. They are initially separated by $10R_R$, starting from 0.43AU. The results in the right panel of Figure 3 clearly show that all embryos undergo rapid orbital decay. This model shows that *the successful assembly of super-critical-mass embryos does not guarantee their retention on a time scale comparable to either the gas accretion or disk depletion time scales.*

For the discussion of several competing processes, we adopt here steady state disk models. They accentuate the potential of resumed migration for embryos with $M_p < M_c$ which failed to evolve into cores. In a subsequent paper, we will investigate embryos' orbital evolution as r_{trans} and M_{opt} decline with Σ_g with \dot{M}_g during the advanced stage of disk evolution.

4. MERGERS AND SUPER-CRITICAL CORES

In this section, we first show that MMR capture may be bypassed in disks with sufficiently large \dot{M}_g ($\gtrsim 10^{-7} M_\odot \text{ yr}^{-1}$). They converge into a compact region (with semi major axis separation $\Delta a < R_f$) where they cross each other's orbits. High accretion rate also obliterates two other growth barriers for embryos with overlapping orbits. These obstacles are 1) large-angle scattering during close encounters, and 2) saturation of corotation torque and resumption of inward migration before cores are able to acquire a mass M_c .

For the active disk simulations, we adopt, in model B, $\dot{M}_g = 10^{-7} M_\odot \text{ yr}^{-1}$. For model B1, we place seven embryos between 5-15.3AU with $M_p = 5M_\oplus$ and $4M_\oplus$ for

the inner two and outer five embryos respectively. These values of M_p 's are comparable to M_{opt} . The embryos' semi major axes are initially separated by $10R_R$. Models A1 and B1 have the same total mass.

4.1. Orbit Crossing and Close Encounters

Embryos migrate on a time scale $\tau_a \sim 2 - 3 \times 10^4$ yr and converge to r_{trans} as their separation is reduced to less than half of their initial spacing (see left panel of Figure 4). The relatively high value $\Sigma(r_{\text{trans}}) > \Sigma(r_{\text{res}})$ (see Eqs. [30], [31] and [32]) enables the embryos to avoid MMR capture.

In such compact configurations, embryos' mutual perturbation excite each other's eccentricity with a growth time scale which decreases rapidly with their separation. Using an idealized disk model in which the Σ_g distribution scales with the minimum mass nebula model, Zhou et al. (2007) estimate that the normalized width of the feeding zone is

$$\log k_{\text{iso}} \simeq (b^2 + 0.61c)^{1/2} - b \quad (33)$$

where $b = 2.8 + 0.33 \log \eta_Z$, $c = 3.6 + 0.67 \log \eta_Z + \log \tau_{\text{dep}}$, $\eta_Z = \eta_d^{3/2} (a/1\text{AU})^{3/4} m_*^{-3/2}$, and η_d is embryos' surface density enhancement factor (relative to the MMN model). Embryos with $\Delta a < k_{\text{iso}} R_R$ undergo orbit crossing within τ_{dep} . For model B1, embryos' Δa is reduced to less than $5R_R$ and their orbits begin to cross within a few 10^4 yr.

After embryos enter each other's feeding zone, they undergo close encounters with impact parameter down to the embryos' radius (R_p) which is $\sim 10^{-4} a$ and < 0.1 times the size of typical computational mesh in hydrodynamic simulations. The Hermite-Embryos scheme is designed and well suited to accurately integrate the orbital evolution associated with these close encounters.

Embryos with overlapping orbits undergo repeated close encounters as they venture into each other's Roche radius. Their eccentricity is excited to $\sim R_R/a$ on a synodic time scale $\tau_{\text{syn}} \sim aP/R_R$. It attains an equilibrium value $\sim (\tau_e/\tau_{\text{syn}})(R_R/a) \sim 0.02 - 0.03$ which is consistent with the left panel of Figure 4. Although the corresponding Safronov number ($\Theta \sim 10^2$) significantly enlarges the embryos' cross section, they scatter many times before any pairs physically collide. In the proximity of r_{trans} , some close encounters lead to large angle deflections, eccentricity excitation and semi major axis spreading. The strength of these perturbations is an increasing function of

$$f_V \equiv V_e(M_{\text{opt}})/V_k(r_{\text{trans}}). \quad (34)$$

Equations (17) and (15) indicate respectively that $M_{\text{opt}} \propto \dot{m}_g^{7/12}$ and $r_{\text{trans}} \propto \dot{m}_g^{0.72}$ so that $f_V \propto \dot{m}_g^{0.5}$. In model B1, close encounters with $f_V < 1$ weakly excite embryos' e 's. Subsequently, *the disk torque not only damps the scattered embryos' eccentricity, but also repatriates them back to the proximity of r_{trans} .*

We highlight these effects with a comparative N-body simulation (in which embryo-disk interaction is neglected). In model B2, we place seven embryos with spatial order but much closer separation (between 6.5-7.8 AU) than model B1. The right panel of Figure 4 show embryos' e are excited from negligible initial values to ~ 0.5 . As a consequence of the close encounters

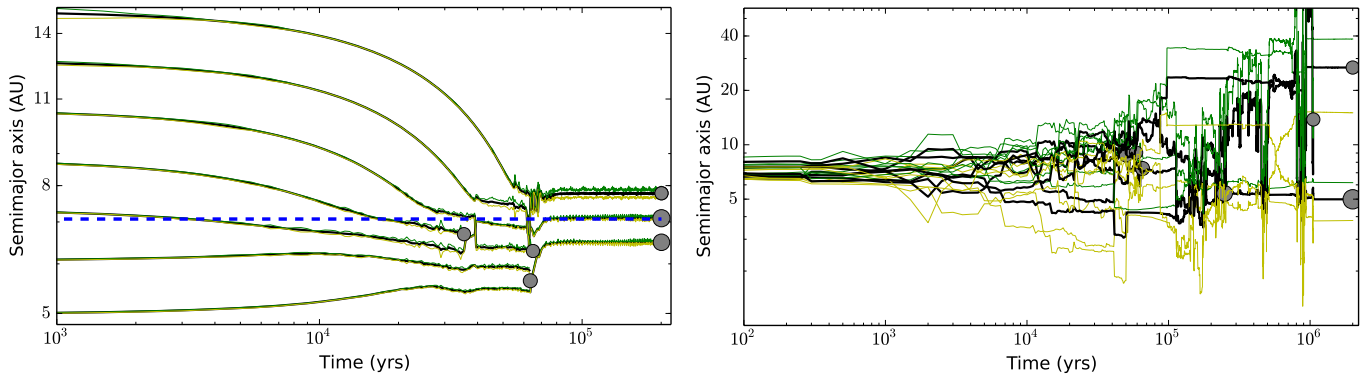


FIG. 4.— The mutual interaction between embryos and their natal disks. The black lines trace the evolution of embryos’ semi-major axis and blue dashed line indicates the location of r_{trap} . Green and yellow lines are embryos’ apocentre and pericentre distance. **Left** model B1: A system of seven embryos including inner two $5M_{\oplus}$ and outer five $4M_{\oplus}$ embryos which are initially separated by $10R_R$ between 5.0 – 15.4AU. Disk parameters are chosen to be those of model B. **Right** model B2: A system of seven embryos including inner two $5M_{\oplus}$ and outer five $4M_{\oplus}$ embryos which are initially separated by $10R_R$ between 6.5 – 7.8AU in the absence of a gaseous disk.

their semi major axes a also become widely separated. Comparison between models B1 and B2 indicates that in disks with sufficiently large Σ_g (and \dot{M}_g), embryos remain congregated near r_{trans} because the embryo-disk torque is effective to damp embryos’ eccentricities e and to repatriate them back to r_{trans} for repeated encounters.

In disks with sufficiently high accretion rate ($\dot{M}_g > 2 \times 10^{-7} M_{\odot} \text{ yr}^{-1}$), r_{trans} exceeds ~ 10 AU where $f_V \gtrsim 1$ for embryos with M_{opt} . Many embryos are episodically scattered into highly elliptical orbits. Even though embryos resume their convergent migration and orbital circularization, this effect significantly prolongs the time scale for embryos to grow through cohesive collisions.

4.2. Embryos’ Collisions

Eventually, the N embryos within Δa , collide and merge on a time scale

$$\tau_c \sim (a\Delta a/NR_p^2)P/2\pi\Theta \quad (35)$$

where $\Theta = GM_p/R_p\sigma^2$ is the Safronov number and $\sigma \sim \Delta a V_k/a$ is the velocity dispersion. For a convoy of a few super Earths with $\Delta a \sim R_R$, $\tau_c \sim 10^4 P$ at $a \sim$ several AU’s. Although τ_c is short compared with the disk lifetime (a few Myr), it is sufficiently long to render 3D hydrodynamic simulation of the merging process impractical. This technical issue is particularly acute for disks with large \dot{M}_g where r_{trap} is at a few AU’s and trapped embryos’ close encounters can significantly enlarge their Δa and prolong their τ_c .

This computational challenge may be partially reduced with 2D simulations of Z14a, Z14b in which τ_c is shortened by a factor of $f_{2/3D} \simeq 1 + \langle i \rangle a/R_p$ where $\langle i \rangle$ is the average inclination of the embryos. We note the enhancement factor would be $a\langle e \rangle/R_p$ if the velocity dispersion is isotropic ($\langle i \rangle \sim \langle e \rangle$) and would be unity if the system is a mono-layer ($\langle i \rangle \sim 0$). However, even in the mono-layer limit, it is impractical to adequately explore the model parameter space and determine the destiny of embryos during the disk evolution.

In our simulations, embryos with overlapping orbits repeatedly undergo close encounters until they physically collide with each other. The first pair of embryos cross each other’s orbits at ~ 7 AU (near r_{trans}) after

$\sim 3.5 \times 10^4$ yr. They then collided with each other within a few hundred periods which is consistent with both the results in Z14b and our estimate of $f_{2/3D}\tau_c$ in equation (35). The magnitude of τ_c is $f_{2/3D} \sim 10^2$ longer in the 3D limit (Rafikov 2004). However, if the embryos’ inclination distribution is damped to that of a mono layer, the 2D estimate would be appropriate. Since both 3D linear analyses (Tanaka et al. 2002) and full 3D hydrodynamic simulations (Bitsch & Kley 2011) indicate the inclination damping timescale is nearly the same order as eccentricity damping timescale, the above assumption is well justified.

Two additional mergers occurred within 7×10^4 yr. The mass of these merger products became comparable to the critical core mass M_c . Two outermost cores captured each other, remained locked in a co-orbital resonance at 7.7AU (left panel of Fig. 4) within 2×10^5 yrs and may eventually merge. The mass of the merger products approaches to the critical value (M_c) for the onset of efficient gas accretion at around 7.1 AU and 6.5 AU.

For embryos with $M_p \sim M_c (\sim 10M_{\oplus})$, $\tau_{\text{KH}} < \tau_{\text{dep}} (\sim 3\text{--}5 \text{ Myr})$. The magnitude of τ_{KH} may be reduced due to an opacity reduction (from its values in the the interstellar medium with solar composition) associated with grain sedimentation in the protoplanetary envelope (Ikoma et al. 2000; Helled & Bodenheimer 2011). Provided the cores’ M_c does not substantially exceed M_{opt} , they are retained near r_{trans} before they gain sufficient mass to open a gap near their a ’s. In model B1, the magnitude of M_{opt} is much larger than that in model A2. In fact, $M_{\text{opt}} \sim M_c$ which implies that cores, once assembled, are more likely to be retained in disks with high \dot{M}_g ’s.

4.3. Trapped Embryos’ Mass Range

Figure 2 indicates that the corotation torque is saturated for small embryos with $M_p < 1M_{\oplus}$ for model A and $M_p < 3.5M_{\oplus}$ for model B. With a uniform α prescription, we carried out simulations with 15 low-mass ($2M_{\oplus}$) embryos (model B) and confirm that they indeed migrate inward, albeit at modest speeds because Γ_0 is relatively smaller for low-mass planets (see eq. [4]).

In §2.3 and §2.4, we indicate that the existence of a dead zone with active surface layers modifies the saturation of the corotation torque. We construct model

C with a set of identical disk structure parameters as those in model B. But in the calculation of f_a , we used a prescription (similar to KL12) in which $\alpha_\nu = \alpha_M$ when $R_R < R_{dz}$ and $\alpha_\nu = \alpha_M + (\alpha_H - \alpha_M) \left(\frac{(R_R/R_{dz})^2 - 1}{(R_R/R_{dz})^2 + 1} \right)$ when $R_H > R_{dz}$. R_R is the planetary Roche radius and the size of dead zone $R_{dz} = H(r)\Sigma_g(r)/\Sigma_\eta$, where $\alpha_H = 10^{-3}$, $\alpha_M = 1.4 \times 10^{-4}$ and Σ_η is a scale value independent of r .

The top panel of Figure 5 indicates that this prescription does not modify r_{trans} but it does enlarge the mass range ($1.5M_\oplus \sim 25M_\oplus$) for the outwardly migrating embryos. In model C1, we place 15 embryos, each with a mass $M_p = 2M_\oplus$ (as in model A1), initially separated by $8R_R$ between 4 and 21.3 AU. In contrast to model B2, embryos initially located at $a < r_{trans}$ migrate outward. They converge with the inwardly migrating embryos on to confined regions with overlapping orbits. Similar to the results in model B1, the first collision (at $\sim 10^5$ yr) was followed by several others. Within $2 - 3 \times 10^5$ yr, seven embryos remain and maximum embryo mass M_p attains $12M_\oplus$ (located at 6.9 AU). In model C1, embryos more massive than M_c can be retained near r_{trans} in contrast to the results in model A2.

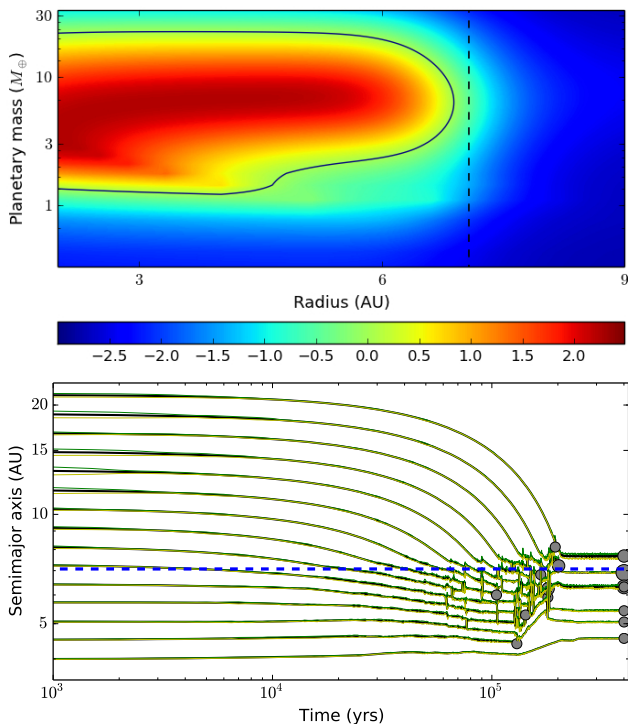


FIG. 5.— **Top:** The type I migration coefficient (f_a) varies with different location and planetary mass at the onset of the simulation for Model C. In this model, the layered structure for the dead zone in the disk is taken into account with a prescription. The disk parameters are chosen the same as those in model B in the right panel of Fig. 2. **Bottom:** Model C1: the dynamical evolution of multiple embryos embedded in above disk model. Fifteen embryos with $2M_\oplus$ are initially separated by $8R_H$ from 4AU to 21.3AU.

5. SUMMARY AND DISCUSSIONS

Gas giant planets are found around 15–20% of nearby solar type stars. In the sequential accretion scenario,

they are formed through gas accretion onto protostellar cores. The accretion rate is determined by the efficiency of radiation transfer through the gaseous envelope. Its associated Kelvin-Helmholtz contraction time is a steeply decreasing function of the cores' mass. Cores can grow into gas giants prior to severe disk depletion only if their mass exceeds a critical value of $10 M_\oplus$.

The assemblage of critical mass (M_c) cores is a crucial step in the formation of gas giant planets. These objects formed through the coagulation of smaller protoplanetary embryos whose oligarchic growth is quenched when they consume all the building block planetesimals in their feeding zone. Embryos' dynamical isolation mass at a few AU in a MMN is a few M_\oplus (Ida & Lin 2004a).

In this paper, we adopt the assumption that migration plays a significant role in dynamical architecture and final fate of planetary systems (Nelson 2005; Alibert et al. 2005; Masset et al. 2006; Paardekooper et al. 2011). We present simulations here to show that one possible mechanism to enlarge the isolation mass is through embryos' extensive type I migration (Lyra et al. 2010; Horn et al. 2012; Hellary & Nelson 2012; Pierens et al. 2013). We constructed a Hermite-Embryo code which includes embryos' interaction with their natal disk and with each other. For the embryo-disk torque, we applied existing prescriptions into a self-consistent disk model.

For the viscously heated inner regions, we show that at its full strength, corotation torque 1) transfers angular momentum from the disk to the embryos at a rate faster than that due to the differential Lindblad torque and 2) induces embryos to migrate outward. However, the corotation torque is saturated (i.e. suppressed) for both relatively high and low mass embryos. For the outer region which is heated by stellar irradiation, embryos generally migrate inward. These embryos converge at the interface between these regions (typically at a few AU's).

Our results indicate that in disks with $\dot{M}_g < 10^{-7} M_\odot \text{ yr}^{-1}$, embryos are caught in their mutual MMR as they slowly approach each other. In this limit, they cannot coagulate and attain the critical mass needed to evolve into gas giants, though they may still accrete a modest envelope. Many of these super Earths are found in multiple systems with a total mass in excess of $10 M_\oplus$. We suggest they are the embryos which failed to attain M_c and evolve into cores. The results in Figure 1 indicate that the minimum total available building block materials around the host stars of most multiple systems are more than adequate to form super critical mass cores. But most of them do not bear signs of gas giant planets. We interpret these data to imply that the lack of gas giants around most solar type stars may be due to the inability for sufficient fraction of all available building block materials to be collected into a few super-critical cores (with $M_p \geq M_c$) rather than a limit supply of heavy elements in their natal disks (Laughlin et al. 2004; Ida & Lin 2004b; Mordasini et al. 2009).

We also show here that embryos' convergent speed increases with the gas accretion rate. In disks with $\dot{M}_g \gtrsim 10^{-7} M_\odot \text{ yr}^{-1}$, embryos congregate with overlapping orbits around a trapping radius outside 7AU. They undergo repeated close encounters while the disk torque damps their excited eccentricity and repatriates them back to the trapping location. The concentration

of embryos elevates their isolation mass and leads to the assemblage of cores.

The threshold criteria ($\dot{M}_d \sim 10^{-7} M_\odot \text{ yr}^{-1}$) is estimated for a steady disk with an assumed $\alpha_\nu \sim 10^{-3}$. This value is consistent with numerical simulations of MRI disks (Sano et al. 2004; Fromang & Nelson 2006) and that inferred from modeling the observed disk accretion rates and masses. We also note that $\sim 20\%$ protostellar disks around T Tauri stars have $\dot{M}_g \gtrsim 10^{-7} M_\odot \text{ yr}^{-1}$. This distribution function provides some support for our conjecture that gas giants around solar type stars are preferentially formed in high- \dot{M}_g disks. All of these estimates are somewhat uncertain.

Different mechanisms have been attributed as the dominant cause of "planet trap" (Masset et al. 2006), including the separatrix of turbulent inner region and outer dead zone (Morbidelli et al. 2008), transition of opacity (Lyra et al. 2010; Bitsch et al. 2013), or transition of dominant energy budget discussed by Kretke & Lin (2012) and this paper. Albeit with some discrepancies, the outward migration mass range and transition radius are universally shown as well. The disk structure promotes the embryos' convergent migration and the accumulating them near different proposed r_{trap} .

Disk models with a broad range of structural parameters including the total disk mass, radial and vertical distribution of viscosity, opacity, accretion rate, detailed energy budget have been applied to hydrodynamical simulations of planet-disk tidal interaction (Bitsch et al. 2013, 2014) and N-body plus additional analytical force simulations (Hellary & Nelson 2012; Pierens et al. 2013) similar to our simulation with the Hermite-Embryo code. Despite the diversity in these disk models, the simulations nevertheless confirm the robustness of embryos' convergent migration process and indicate that embryos' migration history determines whether they evolve into super Earths or cores of gas giant planet.

Hellary & Nelson (2012) simulated the embryos' convergent migration and growth in non-isothermal but somewhat arbitrary chosen disk profile. Pierens et al. (2013) suggested that the resonant convoy can be broken with a large initial number of embryos (total planetary mass in disks) or by including a moderate stochastic force due to the disk turbulence. Although Hellary & Nelson (2012) and Pierens et al. (2013) also mentioned briefly how the disk mass may affect the location of r_{trap} , they did not discuss its influence on the embryos' ability to bypass the MMR. After the submission of this paper, Cossou et al. (2014) posted on Arxiv.org results obtained with a similar approach but a different disk model. In

contrast to the self-consistent steady state disk model (GL07), they assumed a surface density profile and derive a temperature distribution by combining contributions from viscous heating, stellar irradiation and radiative cooling. In their evolving-disk model, opacity and \dot{M} vary with radius and r_{trap} is located near the opacity transition region where the disk temperature gradient is steep. They obtained similar results but did not obtain the quantitative criteria presented here. Another recent paper by Coleman & Nelson (2014) simulated both the formation of cores, gas accretion, and the gas giants' type II migration in evolving disks. Based on their simulation results, they suggested that gas giants formed at large radii in a sufficiently late epoch are preferentially retained. However, many gas giants are observed to reside in multiple-planet systems. Their formation requires adequate residual gas and embryos in their natal disks. The results in Figure 3 (Model A2) indicate that the corotation torque between super Earth cores and low- \dot{M}_g disk is also quenched by saturation. Unless they can induce a gap and a transition to type II migration, these cores would not be retained when the disk gas is severely depleted.

Inspired from the observation (See Figure 1 and the difference between η_J and η_\oplus), our theoretical analysis and numerical simulations places a strong emphasis on that ubiquitous presence of super Earths and limited frequency of gas giants around solar-type stars are the manifestation of a threshold condition which depends on the magnitude of disk accretion rate \dot{M}_g . The results indicate that the embryos must undergo relatively fast convergent migration in order to bypass the MMR barriers and merge into super-critical cores with $M_p > M_c \simeq 10M_\oplus$. Although previous investigations produced similar results for the condition of multiple embryos to overcome resonant barriers, including the dependence of r_{trap} on the disk mass (Hellary & Nelson 2012; Pierens et al. 2013; Cossou et al. 2014), they did not discuss the dependence of the merger probability on the disk mass and accretion rate.

We thank Drs C. Baruteau, S. Ida, K. Kretke, H. Li, and T. Kouwenhoven for useful conversations and an anonymous referee for helpful suggestions to improve the presentation. This work is supported by grants from LDRD, IGPPS from LANL, and UC/Lab Fee's program. B. Liu also thanks T. Kouwenhoven for support with an NSFC grant.

REFERENCES

- Aarseth, S. J. 2003, *Gravitational N-Body Simulations*, ed. Aarseth, S. J.
- Adachi, I., Hayashi, C., & Nakazawa, K. 1976, *Progress of Theoretical Physics*, 56, 1756
- Alibert, Y., Mordasini, C., Benz, W., & Winisdoerffer, C. 2005, *A&A*, 434, 343
- Artymowicz, P. 1993, *ApJ*, 419, 166
- Balbus, S. A., & Hawley, J. F. 1991, *ApJ*, 376, 214
- Balmforth, N. J., & Korycansky, D. G. 2001, *MNRAS*, 326, 833
- Baruteau, C., & Masset, F. 2013, in *Lecture Notes in Physics*, Berlin Springer Verlag, Vol. 861, *Lecture Notes in Physics*, Berlin Springer Verlag, ed. J. Souchay, S. Mathis, & T. Tokieda, 201
- Batalha, N. M., et al. 2013, *ApJS*, 204, 24
- Birnstiel, T., & Andrews, S. M. 2014, *ApJ*, 780, 153
- Bitsch, B., Crida, A., Morbidelli, A., Kley, W., & Dobbs-Dixon, I. 2013, *A&A*, 549, A124
- Bitsch, B., & Kley, W. 2011, *A&A*, 536, A77
- Bitsch, B., Morbidelli, A., Lega, E., & Crida, A. 2014, *A&A*, 564, A135
- Buchhave, L. A., et al. 2012, *Nature*, 486, 375
- . 2014, *Nature*, 509, 593
- Coleman, G. A. L., & Nelson, R. P. 2014, *MNRAS*, 445, 479
- Cossou, C., Raymond, S. N., Hersant, F., & Pierens, A. 2014, *ArXiv e-prints*
- Cumming, A., Butler, R. P., Marcy, G. W., Vogt, S. S., Wright, J. T., & Fischer, D. A. 2008, *PASP*, 120, 531
- Dong, S., & Zhu, Z. 2013, *ApJ*, 778, 53

- Dullemond, C. P., & Dominik, C. 2005, *A&A*, 434, 971
 Fischer, D. A., & Valenti, J. 2005, *ApJ*, 622, 1102
 Fressin, F., et al. 2013, *ApJ*, 766, 81
 Fromang, S., & Nelson, R. P. 2006, *A&A*, 457, 343
 Gammie, C. F. 1996, *ApJ*, 457, 355
 Garaud, P., & Lin, D. N. C. 2004, *ApJ*, 608, 1050
 —. 2007, *ApJ*, 654, 606
 Garaud, P., Meru, F., Galvagni, M., & Olczak, C. 2013, *ApJ*, 764, 146
 Goldreich, P., & Sari, R. 2003, *ApJ*, 585, 1024
 Goldreich, P., & Tremaine, S. 1979, *ApJ*, 233, 857
 —. 1980, *ApJ*, 241, 425
 Goldreich, P., & Ward, W. R. 1973, *ApJ*, 183, 1051
 Hartmann, L., Calvet, N., Gullbring, E., & D'Alessio, P. 1998, *ApJ*, 495, 385
 Hayashi, C. 1981, *Progress of Theoretical Physics Supplement*, 70, 35
 Hellary, P., & Nelson, R. P. 2012, *MNRAS*, 419, 2737
 Helled, R., & Bodenheimer, P. 2011, *Icarus*, 211, 939
 Horn, B., Lyra, W., Mac Low, M.-M., & Sándor, Z. 2012, *ApJ*, 750, 34
 Howard, A. W., et al. 2012, *ApJS*, 201, 15
 Ida, S., & Lin, D. N. C. 2004a, *ApJ*, 604, 388
 —. 2004b, *ApJ*, 616, 567
 Ikoma, M., Nakazawa, K., & Emori, H. 2000, *ApJ*, 537, 1013
 Johansen, A., & Youdin, A. 2007, *ApJ*, 662, 627
 Johnson, J. A., Aller, K. M., Howard, A. W., & Crepp, J. R. 2010, *PASP*, 122, 905
 Kenyon, S. J., & Bromley, B. C. 2009, *ApJ*, 690, L140
 Kley, W., & Nelson, R. P. 2012, *ARA&A*, 50, 211
 Kokubo, E., & Ida, S. 1998, *Icarus*, 131, 171
 Kretke, K. A., & Lin, D. N. C. 2012, *ApJ*, 755, 74
 Lambrechts, M., & Johansen, A. 2012, *A&A*, 544, A32
 Laughlin, G., Bodenheimer, P., & Adams, F. C. 2004, *ApJ*, 612, L73
 Leinhardt, Z. M., & Richardson, D. C. 2005, *ApJ*, 625, 427
 Lin, D. N. C., & Papaloizou, J. 1986a, *ApJ*, 307, 395
 —. 1986b, *ApJ*, 309, 846
 Lin, D. N. C., & Papaloizou, J. C. B. 1993, in *Protostars and Planets III*, ed. E. H. Levy & J. I. Lunine, 749–835
 Lissauer, J. J. 1987, *Icarus*, 69, 249
 Lissauer, J. J., et al. 2011, *ApJS*, 197, 8
 —. 2012, *ApJ*, 750, 112
 Lynden-Bell, D., & Pringle, J. E. 1974, *MNRAS*, 168, 603
 Lyra, W., Paardekooper, S.-J., & Mac Low, M.-M. 2010, *ApJ*, 715, L68
 Marcy, G. W., et al. 2008, *Physica Scripta Volume T*, 130, 014001
 —. 2014, *ApJS*, 210, 20
 Masset, F. S. 2001, *ApJ*, 558, 453
 Masset, F. S., Morbidelli, A., Crida, A., & Ferreira, J. 2006, *ApJ*, 642, 478
 Mayor, M., et al. 2011, *ArXiv e-prints*
 Morbidelli, A., Crida, A., Masset, F., & Nelson, R. P. 2008, *A&A*, 478, 929
 Mordasini, C., Alibert, Y., & Benz, W. 2009, *A&A*, 501, 1139
 Murray, C. D., & Dermott, S. F. 1999, *Solar system dynamics*
 Nelson, R. P. 2005, *A&A*, 443, 1067
 Paardekooper, S.-J., Baruteau, C., Crida, A., & Kley, W. 2010, *MNRAS*, 401, 1950
 Paardekooper, S.-J., Baruteau, C., & Kley, W. 2011, *MNRAS*, 410, 293
 Peale, S. J. 1976, *ARA&A*, 14, 215
 Pierens, A., Cossou, C., & Raymond, S. N. 2013, *A&A*, 558, A105
 Pollack, J. B., Hubickyj, O., Bodenheimer, P., Lissauer, J. J., Podolak, M., & Greenzweig, Y. 1996, *Icarus*, 124, 62
 Pringle, J. E. 1981, *ARA&A*, 19, 137
 Rafikov, R. R. 2004, *AJ*, 128, 1348
 Ruden, S. P., & Lin, D. N. C. 1986, *ApJ*, 308, 883
 Sano, T., Inutsuka, S.-i., Turner, N. J., & Stone, J. M. 2004, *ApJ*, 605, 321
 Santos, N. C., Israelian, G., & Mayor, M. 2004, *A&A*, 415, 1153
 Schneider, J., Dedieu, C., Le Sidaner, P., Savalle, R., & Zolotukhin, I. 2011, *A&A*, 532, A79
 Shakura, N. I., & Sunyaev, R. A. 1973, *A&A*, 24, 337
 Stewart, S. T., & Leinhardt, Z. M. 2009, *ApJ*, 691, L133
 Tanaka, H., Takeuchi, T., & Ward, W. R. 2002, *ApJ*, 565, 1257
 Wang, J., & Fischer, D. A. 2013, *ArXiv e-prints*
 Weidenschilling, S. J., & Cuzzi, J. N. 1993, in *Protostars and Planets III*, ed. E. H. Levy & J. I. Lunine, 1031–1060
 Wolfgang, A., & Lopez, E. 2014, *ArXiv e-prints*
 Wright, J. T., et al. 2011, *PASP*, 123, 412
 Wu, Y., & Lithwick, Y. 2013, *ApJ*, 772, 74
 Youdin, A. N., & Goodman, J. 2005, *ApJ*, 620, 459
 Youdin, A. N., & Shu, F. H. 2002, *ApJ*, 580, 494
 Zhang, X., Li, H., Li, S., & Lin, D. N. C. 2014a, *ApJ*, 789, L23
 Zhang, X. J., Liu, B. B., & Lin, D. N. C. 2014b, *ApJ* in press.
 Zhou, J.-L., Lin, D. N. C., & Sun, Y.-S. 2007, *ApJ*, 666, 423